

The unconstrained evolution of fast and efficient antibiotic-resistant bacterial genomes

Carlos Reding-Roman, Mark Hewlett[†], Sarah Duxbury[†], Fabio Gori, Ivana Gudelj and Robert Beardmore*

Evolutionary trajectories are constrained by trade-offs when mutations that benefit one life history trait incur fitness costs in other traits. As resistance to tetracycline antibiotics by increased efflux can be associated with an increase in length of the *Escherichia coli* chromosome of 10% or more, we sought costs of resistance associated with doxycycline. However, it was difficult to identify any because the growth rate (r), carrying capacity (K) and drug efflux rate of *E. coli* increased during evolutionary experiments where the species was exposed to doxycycline. Moreover, these improvements remained following drug withdrawal. We sought mechanisms for this seemingly unconstrained adaptation, particularly as these traits ought to trade-off according to rK selection theory. Using prokaryote and eukaryote microorganisms, including clinical pathogens, we show that r and K can trade-off, but need not, because of ' rK trade-ups'. r and K trade-off only in sufficiently carbon-rich environments where growth is inefficient. We then used *E. coli* ribosomal RNA (rRNA) knockouts to determine specific mutations, namely changes in rRNA operon (*rrn*) copy number, than can simultaneously maximize r and K . The optimal genome has fewer operons, and therefore fewer functional ribosomes, than the ancestral strain. It is, therefore, unsurprising for r -adaptation in the presence of a ribosome-inhibiting antibiotic, doxycycline, to also increase population size. We found two costs for this improvement: an elongated lag phase and the loss of stress protection genes.

Trade-offs lie at the heart of a cross-kingdom research effort that seeks to explain how biodiversity is generated and maintained^{1–5}. Two traits engage in an evolutionary trade-off when beneficial mutations to one trait are deleterious to the other, and vice versa, and many theories agree^{2,6–11} that genetic polymorphisms are maintained when trade-offs have an appropriate geometry. Less clear, however, are the physical, chemical and physiological forces that create trade-offs in the first place¹², and trade-offs needed for the theories to work can be difficult to isolate in practice^{13–18}.

It is essential for medicine that we understand trade-offs. The term ‘superbug’ refers to a pathogenic microorganism that resists treatment by antibiotics with no apparent cost, or trade-off, in terms of its pathogenicity. An evolutionary route to superbug status is thought to occur when a pathogen first adopts costly drug resistance mutations, a process that sees resistance traded against proliferation rate in antibiotic-free environments. Thereafter, other mutations compensate for those costs, yielding strains that are both drug resistant and capable of rapid proliferation^{19,20}.

Trade-offs have been observed in pathogens. A genomic study of a clinical pathogen using several antibiotic classes²¹ showed resistance costs were dynamic during treatment for a *Salmonella* infection in which drug efflux proteins exhibited between-drug trade-offs. During treatment, structural mutations that increased efflux rates for one antibiotic decreased them for others. Biophysical trade-offs like this are important as they can help support genetic diversity, as was shown in a laboratory study where the rate-affinity trade-off maintained a trimorphic transporter gene in a bacterial population¹⁰.

Single-protein trade-off mechanisms, such as the above, are more readily identified than organism-wide trade-offs, where costs may be hard to discern. Indeed, a classical concept, the rK

trade-off, where r is growth rate and K is organismal carrying capacity, suffers from an absence of both mechanism and data, and so, along with rK selection theory, fell out of favour some time ago²². Others argue that rK theory is relevant to understanding tumour progression and heterogeneity^{23,24}, but details of how rK selection theory makes predictive statements about tumour evolution are unclear. Interestingly, much the same can be said of the rate–yield trade-off (RYTO) postulated for microorganisms and cancers²⁵ that has also proved elusive^{14,26–28}. Here ‘rate’ refers to growth rate and ‘yield’ to a metabolic conversion efficiency, c , between carbon source intake and biomass production. Some have observed a RYTO¹⁰, whereas others have seen weak RYTOs or no trade-off at all; even positive rate–yield correlations have been observed^{13,26,27} (that is, a trade-up).

In this study of *Escherichia coli* and fungal *Candida* we, too, see both rK and rate–yield trade-offs and trade-ups. However, we show that this is only to be expected mechanistically because, for unicellular organisms, rK and rate–yield relationships derive from one underlying theory. By applying that theory, which is consistent with all our data, we resolve the geometry of the RYTO by demonstrating it has a parabolic shape that contains a trade-up. As a direct corollary, we also resolve the geometry of rK trade-offs for microorganisms, including *Candida*, by showing that it, too, has a parabolic shape where growth rate is maximal at intermediate population size.

The presence of rK trade-ups is important for antibiotics that suppress r and K by design, which the antibiotic doxycycline achieves by slowing protein production in *E. coli*. Antibiotic resistance mutations should restore r during chemotherapy but, here, the absence of rK constraints during resistance evolution allows the creation of a seemingly *E. coli* mutant ‘überbug’ that effluxes

Biosciences, Geoffrey Pope, University of Exeter, Stocker Road, Exeter EX4 4QD, UK. [†]These authors contributed equally to this work.
*e-mail: r.e.beardmore@exeter.ac.uk

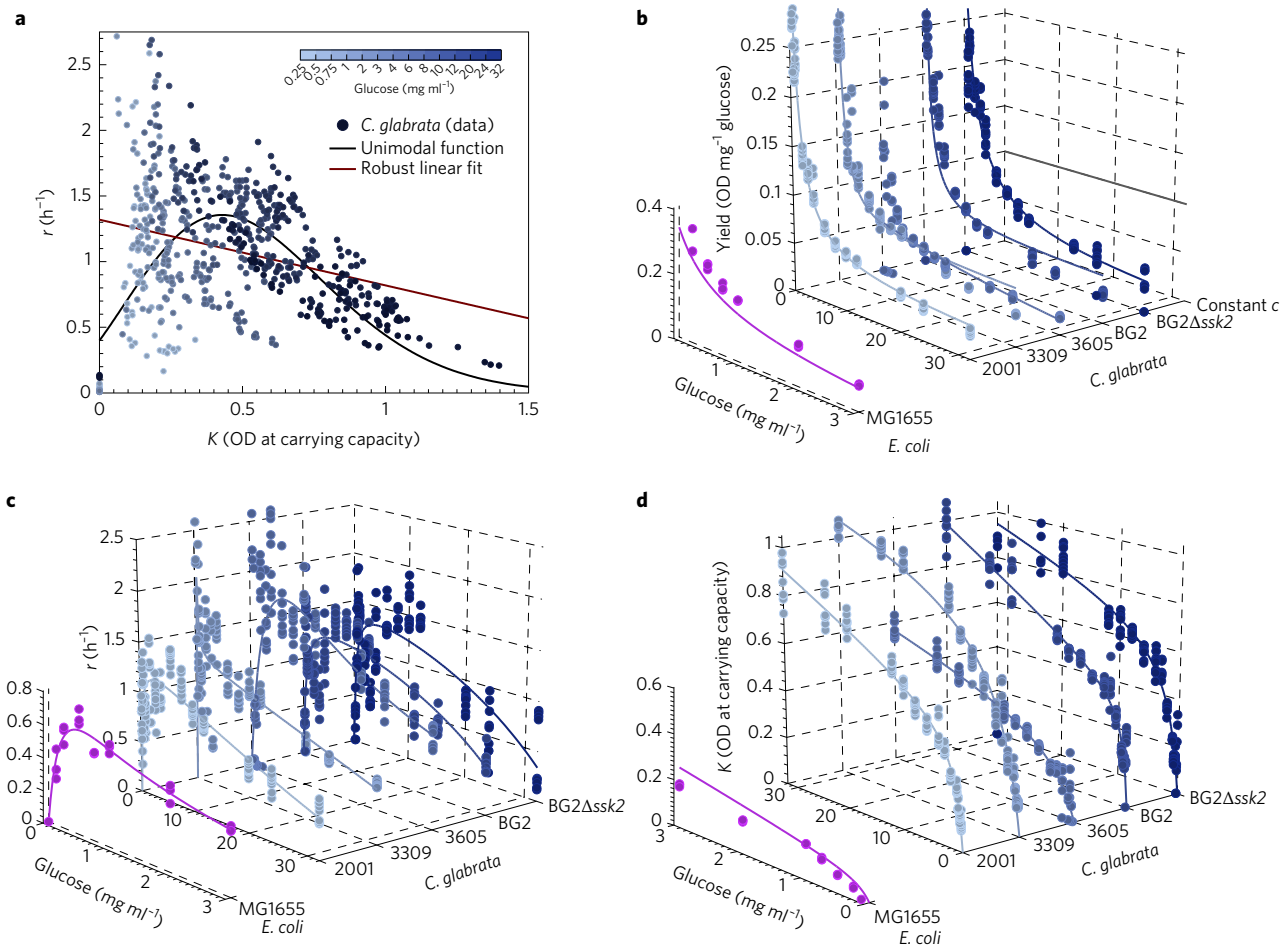


Figure 1 | Collated rK data sets are best explained by unimodal data fits; K , r and yield data sets in fungi and bacteria are explained by equations (2)–(7).

a, Collated growth rates (r) from different *C. glabrata* strains on the y axis and population size (K) on the x axis; each data point has a corresponding glucose supply concentration. A unimodal regression based on a scaled Poisson distribution function ($r(K) = p \times \exp(n \times \ln K - K - \Gamma(n+1))$ where p and n are shape parameters, Γ is the gamma function) and a robust linear regression are shown. Based on the corrected Akaike information coefficient, AIC_c , the relative likelihood of the two regressions is $<10^{-15}$: the unimodal fit is significantly more likely. **b**, Biomass per milligram of glucose supplied (that is, yield) on the z axis for *C. glabrata* and *E. coli*, with glucose supply on the x axis and strain labels on the y axis. Data points are dots whereas predictions from equation (5) are lines (adjusted $R^2 \approx \{0.995, 0.98, 0.99, 0.95, 0.98\}$ for the *Candida* strains). **c,d**, Analogously, r (**c**) and K (**d**) are shown on the z axis, indicating their dependence on the supply of glucose (x axis). Model predictions (solid lines) are obtained by fitting equations (2)–(7) to data using NonLinearModel.fit in Matlab.

doxycycline more quickly and grows more rapidly to higher densities than its wild-type (WT) ancestor, whether or not the antibiotic is present. We were able to isolate one phenotypic and one genetic cost to this triple improvement: increased delay in the onset of exponential growth and the loss of stress protection genes contained in a prophage.

Results

We first present a mechanistic argument¹⁰ supporting a parabolic relationship between growth rate in the exponential phase of microorganisms and the population size that those microorganisms achieve; recent extensions of flux balance analysis provide another argument²⁹. As a result of the parabolic geometry of this trait pairing, rK relationships can contain both trade-ups and trade-offs.

First, consider the rK trade-up: it is straightforward to see why r and K might be positively correlated. Assume a carbohydrate, such as glucose, is a limiting source of carbon, as can be the case for tumours and microorganisms. The size of a population of unicellular organisms can be predicted from the carbohydrate

concentration if the number of cells produced per carbon molecule (that is, yield), c , is a constant:

$$\begin{aligned} K &= \frac{\text{yield } (c)}{\text{number of cells}} \\ &= \frac{\text{yield } (c)}{\text{moles of available glucose}} \times \text{moles of available glucose} \\ &= c \times S \end{aligned} \quad (1)$$

where S is the concentration of that extracellular carbohydrate. Equation (1) circumvents one problem of rK theory in which ' K ' cannot be realistically expressed as a function of life history traits³⁰. Equation (1) addresses this for microorganisms whereby the trait is yield, c , which is multiplied by the available nutrient to form K ³¹. However, equation (1) will not apply to multicellular organisms, in which different cells in tissue develop with different nutrient-to-biomass conversion efficiencies.

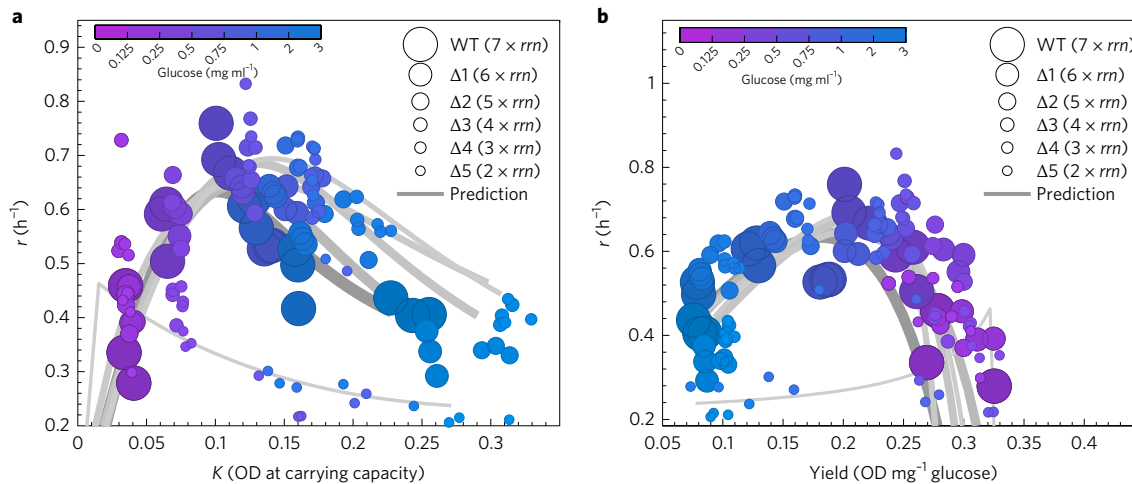


Figure 2 | Empirical and theoretic rK and r -yield relationships. **a,b,** Empirical and theoretic rK relationships (**a**) and r -yield relationships (**b**); dots are data, solid lines are theoretical model fits. Consistent with theory, these are skewed parabolae for all the strains of *E. coli* K12(MG1655) WT and *rrn* knockout strains used in this study, except for the one with fewest *rrn* operons. The strain with only two such operons (smallest dots shown) does not conform to this geometry and, unlike the other strains, has an rK trade-off with no trade-up region.

To relate growth rate to the carbohydrate, assume for now that r varies as a Monod function³¹:

$$r = r(S) = c \times \frac{V_{\max}S}{k_m + S} \quad (2)$$

where k_m is a half-saturation parameter, so-called because $r(k_m) = \frac{1}{2}\max[r(S):S \geq 0]$ and V_{\max} is the maximal uptake rate of carbohydrate into the cell. As $S = K/c$ in equation (1), using equation (2), we derive a putative rK relationship:

$$r = r(K/c) = c \times \frac{V_{\max} \times K}{k_m \times c + K} \quad (3)$$

Equation (3) is consistent with microbial data³¹ but, interestingly, inconsistent with classical rK theory: increasing r increases K . Assumptions typical of rK theory^{32,33}, for example that a linear regression $r = a - bK$ can describe rK data sets, are not compatible with equation (3). To resolve this for microorganisms, we first turn to a clinical pathogen, *Candida glabrata*.

RYTO and rK relationships in *C. glabrata*. By culturing (see Methods) *C. glabrata* in media with different concentrations of glucose as the carbon source, seeking to test equations (1)–(3) against data, we determined the dependence of r and K on glucose supply. Figure 1a summarizes this data set and the Methods section details how r and K are determined from microbial culture data. It shows a linear regression poorly captures the data (parameter-adjusted $R^2 \approx 0.13$), so does equation (3) (adjusted $R^2 \approx 0.46$), and a unimodal Poisson distribution function is a marginally better fit (adjusted $R^2 \approx 0.48$). One might hypothesize, from Fig. 1a, that equation (3) and a linear regression apply to different subsets of the data: equation (3) applies at low K , whereas data are approximately linear at high K . Much better would be one theory capturing all the data.

For this, we summarize a calculation performed elsewhere^{10,34} that removes the assumption in equation (2) that yield, c , is a constant independent of environment^{10,34} by writing

$$K = \text{number of cells} = \frac{\text{cells}}{\text{ATP}} \times \overbrace{\frac{\text{ATP}}{\text{glucose}}}^{\text{S-dependent}} \times \text{glucose} \quad (4)$$

$$= c(A) \times A(S) \times S$$

We now need information about two measures of efficiency: the adenosine tri-phosphate (ATP) produced per cell $c(A)$, and the ATP per glucose in each cell $A(S)$. To allow progress, although not ideal, we now assume that ATP per cell does not depend on glucose availability. This allows yield, $c(S)$, to depend only on glucose concentration, S . This is the simplest possible extension we could make to add realism to equations (2) and (3).

It has been shown¹⁰, to approximation, that

$$c(S) = c_{hi} \frac{1}{1 + pS} + \frac{pS}{1 + pS} c_{lo} \quad (5)$$

where p is a shape parameter, c_{lo} is the lowest possible yield and c_{hi} is the highest possible yield over a non-toxic range of carbohydrate concentrations; Fig. 1c validates equation (5) for *Candida* and *E. coli*. If we modify equations (2) and (3) to accommodate equation (5), we then obtain a curve in the rK -plane parameterized by S :

$$(r, K) = (r(S), K(S)) = \left[c_{hi} \frac{1}{1 + pS} + \frac{pS}{1 + pS} c_{lo} \right] \times \left(\frac{V_{\max}S}{k_m + S}, S \right) \quad (6)$$

where $K(S) = S \times c(S)$. Equation (6) can be written as a rate–yield relationship^{10,25–27,34}. To see this, divide $K(S)$ by S to form $c(S)$:

$$(r, c) = (r(S), c(S)) = \left[c_{hi} \frac{1}{1 + pS} + \frac{pS}{1 + pS} c_{lo} \right] \times \left(\frac{V_{\max}S}{k_m + S}, 1 \right) \quad (7)$$

Supplementary Fig. S3 illustrates geometric trade-up and trade-off forms described by equations (5)–(7). Note that we cannot fit equations (6) and (7) directly to rK and rate–yield data. Instead, to obtain those data, we first determine p , c_{lo} and c_{hi} from yields determined at different carbohydrate concentrations. We then determine k_m and V_{\max} from r data measured at different carbohydrate concentrations.

Let us test this reasoning on *C. glabrata* rK data. Figure 1b–d shows that equation (5) is an excellent descriptor of *C. glabrata* yield (adjusted $R^2 \approx 0.995, 0.98, 0.99, 0.95, 0.98$ for five strains). We then eliminated parameters V_{\max} and k_m in equation (6) using those data and the resulting data fits and—this is key—exhibit unimodal, parabola-like profiles (Fig. 1 and Supplementary Figs S5,

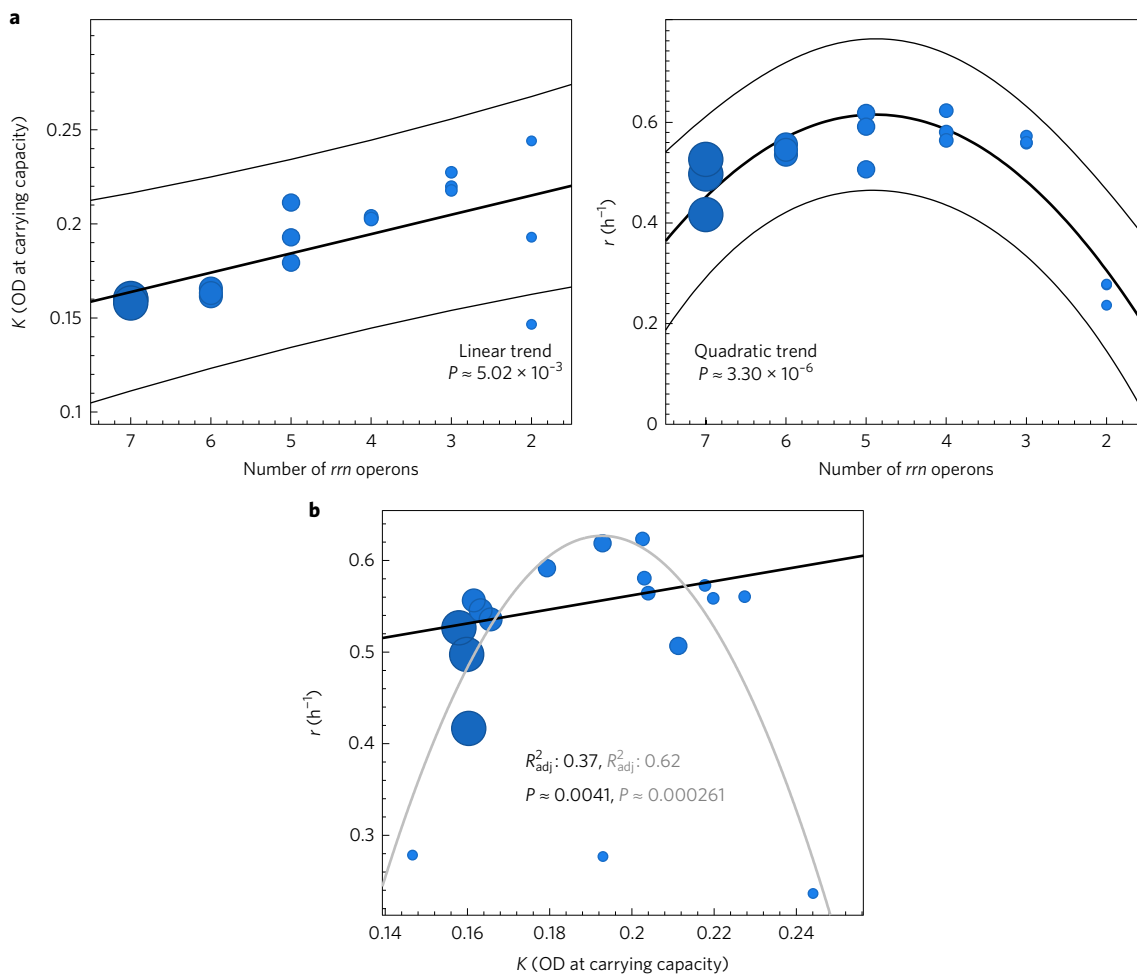


Figure 3 | A demonstration that *rrn* operon copy number controls *r* and *K* by mediating yield: to turn *K* into yield, divide by 2 mg ml⁻¹ glucose.

a, Relationship between the number of *rrn* operons, carrying capacity (*K*, left panel) and growth rate (*r*, right panel) for one glucose concentration (2 mg ml⁻¹; Fig. 4 and Supplementary Fig. 8 contain more). Linear and quadratic regressions are shown, respectively, as lines \pm estimated 95% confidence intervals (CI; three replicates). These data indicate greater *K* results from fewer operons for fixed glucose supply and that *r* can be maximized at intermediate operon number. **b**, Scatterplot of collated (*r*, *K*) values for all *rrn* knockout strains for one glucose concentration showing a quadratic relationship is a better descriptor of data than a linear regression; note, this also serves as a between-genotype rate–yield plot. The size of the dot for each datum corresponds to *rrn* operon number, as per **a**.

S3 and S4) in which *r* exhibits its maximum at intermediate *K*. Thus, equation (6) reconciles the competing trade-off and the Monod-based, trade-up theories of *rK* data. Furthermore, the fit of equation (7) to *C. glabrata* rate–yield data is unimodal in rate and yield (Supplementary Fig. S4). This is consistent with previous, untested predictions on the shape of the RYTO²⁵ that are corroborated by recent flux balance analyses²⁹.

Figure 1 shows the dependence of *r*, yield and *K* on *S* for five *C. glabrata* strains. This shows *K* increases nonlinearly as glucose supply increases due to a decrease in efficiency at high, non-toxic glucose concentrations (relative likelihood of linear and a nonlinear regression $<10^{-16}$), a property not observed by Monod³¹. As a result, growth rate can decrease as glucose supply increases (Fig. 1c), and so growth rate can be maximized at intermediate glucose concentrations.

Given differences in their blood sugar levels, we sought, and found, evidence for different *rK* and rate–yield profiles in the fungal infections of diabetic and non-diabetic patients. Supplementary Fig. S5a compares *rK* parabolae of *C. glabrata* strains 2001 and 3605, the latter isolated from a diabetic patient, which indicate a between-strain *rK* trade-off: 2001 has lower *r* with potential for greater *K* than does 3605 (*t*-test for *r*: $t \approx -4.52$, d.f. = 250, $P < 10^{-5}$; for *K*: $t \approx 7.72$, d.f. = 250, $P < 10^{-12}$). Supplementary Fig. S5b shows

the mathematical *rK* model data fit for the *C. glabrata* strain taken from a diabetic patient has a skewed profile towards higher growth rates at lower population densities.

RYTO and *rK* relationships in *E. coli*. We then asked whether the parabolic *rK* shape was specific to eukaryotes. It is not, Fig. 2 shows *E. coli* has *rK* parabolae too. We use *E. coli* strains MG1655, WT, $\Delta 1$ and $\Delta 2-\Delta 5$ that have different numbers of rRNA operons (*rrn*) in their genomes; WT has 7, $\Delta 1$ has 6, $\Delta 2$ has 5, and so on. Figure 1 and Supplementary Fig. S5 show that the claims made above for *Candida* apply equally to these *E. coli*, and Fig. 2 shows the RYTO and *rK* shapes to be robust to changes in the number of *rrn* operons. These *E. coli* answer the following question: do genetic changes that increase yield, and therefore *K*, lead to a concomitant decrease in *r*? In other words, can we produce evidence of a between-strain *rK* trade-off?

In response, rRNA is known to constitute a metabolic burden under carbon limitation^{35,36}. By using these *E. coli* strains whereby this burden is under genetic control, we can mediate *r* and yield, thus *K*, to probe how selection for one of these traits affects the others. To this end, we establish the following property of the six *E. coli* strains that differ in the number of *rrn* operons. First, strains with

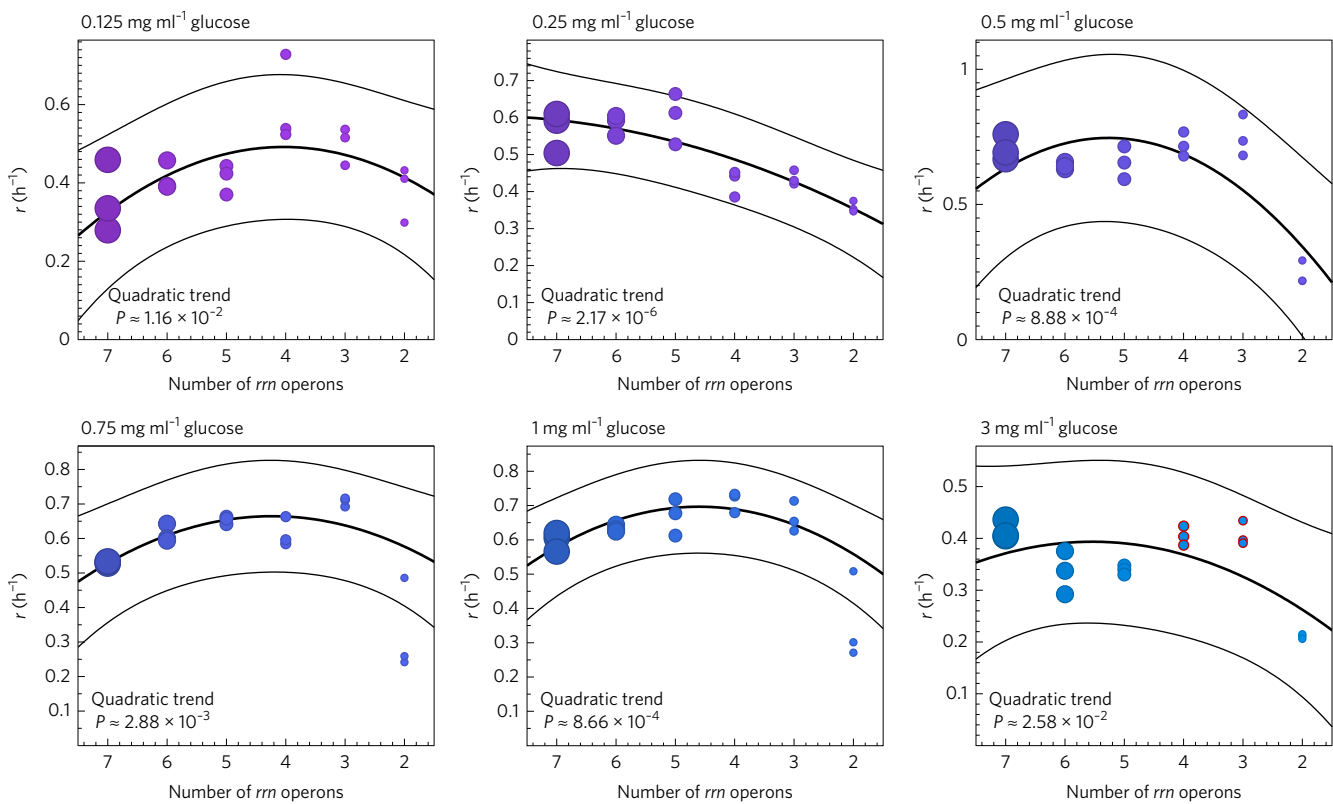


Figure 4 | Determining the *rrn* operon copy number that maximizes growth rate of the *E. coli rrn* mutants. Growth rate (r) is shown on the y axis as a function of *rrn* operon copy number (x axis) for different glucose supply concentrations. We sought a relationship between growth rate and operon copy number using linear and quadratic regressions, and plotted the regression with the better fit to data according to adjusted R^2 value (solid black line; outer lines are the prediction \pm 95% CI). These data indicate that intermediate *rrn* operon numbers can optimize r under some environmental conditions, although higher numbers of operons (the wild-type *E. coli* strain has seven) can also optimize r under other conditions. For completeness, using the quadratic regression we computed 95% CI for r -optimal *rrn* copy numbers for $\{0.5, 0.75, 1, 2, 3\} \text{ mg ml}^{-1}$ glucose; these are, respectively, $\{5.26 \pm 0.47, 4.22 \pm 0.24, 4.60 \pm 0.02, 4.89 \pm 0.11, 5.53 \pm 1.21\}$. This shows that seven operons is not optimal for growth under all environmental conditions, although it is optimal for some (0.25 and 3 mg ml⁻¹ glucose). Red dots in the bottom right panel indicate populations that optimize K from all glucose concentrations tested.

fewer such operons have greater yields at the same carbon supply concentrations, and subsequently higher K (Fig. 3a; Supplementary Fig. S8 shows P values). According to equation (7), the number of *rrn* operons, as they mediate yield, should also mediate r , and indeed they do (Figs 3a and 4). This operon also mediates lag phase (Supplementary Fig. S11). We thus have three inter-dependent traits, r , K and yield under genetic control, as desired, and lag phase too.

Figure 4 shows that different copy numbers of *rrn* optimize r at different glucose availabilities, although yield (therefore K) is optimized when fewest operons are present (Supplementary Fig. S8). Figure 3b and Supplementary Fig. S9 show there is no between-genotype RYTO between these strains because changes in *rrn* copy number can follow a parabolic geometry exhibiting both positive and negative corrections with r and K , and that which occurs is contingent on the glucose available. Supplementary Fig. S7 summarizes this information using three empirical and theoretical r , yield and K landscapes illustrating the dependence of these phenotypes on glucose and *rrn* operon number.

Data from the *E. coli* strain set indicate it may be possible to simultaneously improve r and K by mutational change, for example by deleting or duplicating an *rrn*, but is it? To answer this, we sought genetic and environmental conditions where population size is largest and Fig. 5a provides a self-evident response: K is largest at greatest nutrient supply, as is obvious, and for the highest yield genomes, namely when *rrn* copy number is low. Now, Fig. 5a,b shows that the strain with 3 and 4 *rrn* operons resides within a

two-strain cluster with maximal K but that also has the largest observed r (Supplementary Clustering Analysis). Finally, Fig. 5c shows that rate and yield, and therefore K , can be positively or negatively correlated between genotypes, depending on the glucose background in which growth takes place. We conclude that improvements in K are not associated with a penalty in r in this strain set: deleting operons from the WT can improve both r and K .

***E. coli* rate–yield and rK changes following adaptation to an antibiotic.** K , r and yield phenotypes are relevant to clinical infections because some antibiotics, those said to be bacteriostatic, explicitly reduce r without lysing cells in a way that would reduce K . We therefore ask: do drug-resistance mutations that restore r during a bacteriostatic antibiotic challenge also reduce yield or K ? Previous RYTO and rK theory would predict so. However, the potential for rK and rate–yield trade-offs demonstrated above indicates that some resistance mutations might, instead, increase both r and K .

To study this, we propagated six replicate *E. coli* K12 (AG100) populations for 4 days of antibiotic treatment at clinical levels above the minimal inhibitory concentration (MIC) of doxycycline treating every 12 h with drug (~60 generations, MIC from 24 h data in Supplementary Fig. S12, see Methods). Figure 6 summarizes the resulting r and K phenotypes. First, r in the presence of drug was restored to, and greater than, that of the ancestral strain in the absence of drug (Fig. 6b, $P < 0.012$, d.f. = 6, $t \approx -3.5$). However, discordant with the hypothesis of a RYTO or rK trade-off during adaptation, K also increased above that observed in both the

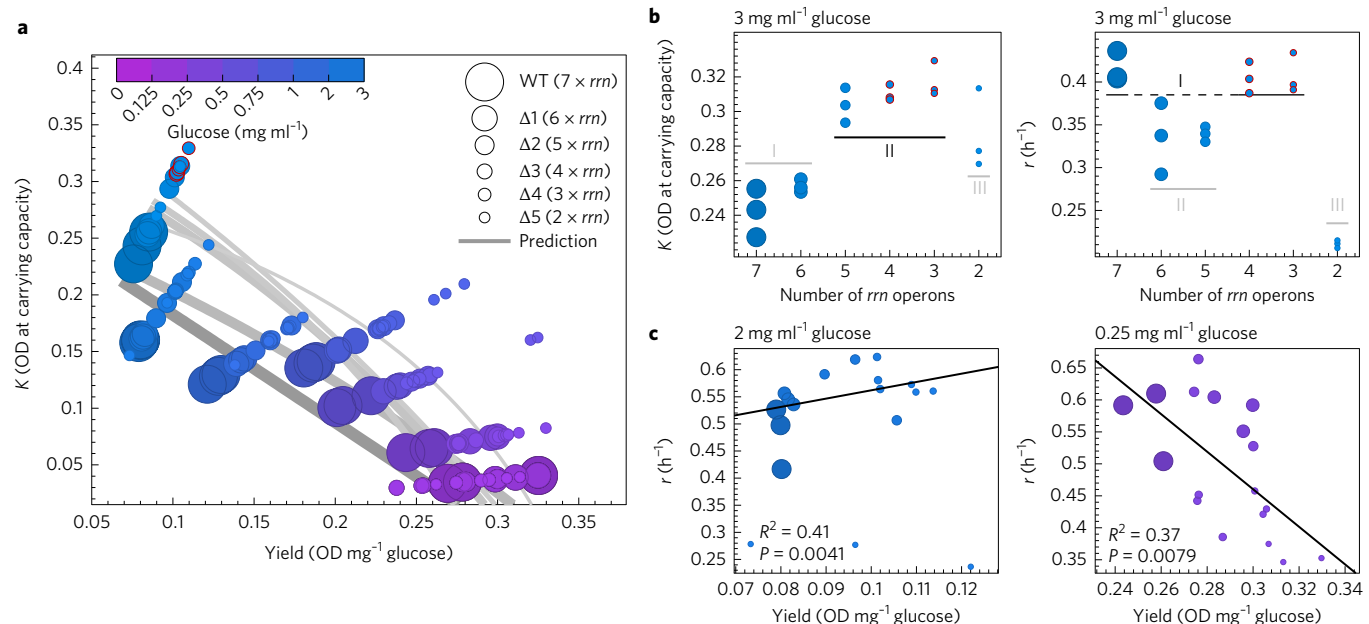


Figure 5 | *E. coli* K12(MG1655) *rrn* knockout strains $\Delta 3$ and $\Delta 4$ optimize population size, K , when glucose is high in concentration without paying a growth rate cost. **a**, Empirical data (dots) and theoretical predictions (lines using models in main text) for each *rrn* knockout strain show the variation in K (y axis) as a function of yield (x axis) and *rrn* operon copy number (dot size). The cluster of combinations of *rrn* operon number and glucose supply concentration that maximize K are highlighted as red dots: self-evidently, K is greatest when glucose supply is greatest and growth is efficient, meaning few *rrn* operons (see Supplementary Fig. S8). As $K/\text{yield} = \text{glucose concentration}$, when glucose concentration is fixed, the collated data for all strains lie on straight lines that pass through $(\text{yield}, K) = (0, 0)$. The highest yield outcome is marked as a large red circle: the WT strain cultured at the lowest glucose concentration. **b**, An agglomerative, one-dimensional clustering analysis (Supplementary Methods) shows that the highest population sizes found at the highest glucose concentration tested (K -cluster II, shown left) are also achieved at the highest observed growth rates (r -cluster I, shown right). As a result, operon copy numbers that simultaneously optimize r and K are highlighted with red circles (three and four copies of *rrn*). **c**, There is no between-strain trade-off in r and K : dot sizes indicate different *rrn* copy number (as Fig. 2) with each datum representing observed r and K at high (left) and low (left) glucose concentration. Linear regressions (black lines) indicate that r and K can be both positively and negatively correlated, depending on the environment (Supplementary Fig. S9 shows more glucose concentrations).

ancestral strain and in the strain adapted to growth media containing no doxycycline (K nearly tripled: Fig. 6a, $P \approx 1.3 \times 10^{-7}$, d.f. = 6, $t \approx -28.1$ for the 'Ancestral' strain; $P \approx 4.0 \times 10^{-7}$, d.f. = 6, $t \approx -23.4$ for the 'Media Adapted' strain). Thus, although it was an antibiotic molecule for initial treatments, doxycycline eventually stimulated biomass production. Supplementary Figs S12 and S14 show that doxycycline can also stimulate population growth within 48 h at near MIC dosages.

Simultaneous rK improvements in AG100 were observed not only at super-MIC dosages, they also arose when the same adaptation protocol was performed at sub-MIC dosages (see Methods). In this case, populations that had been inhibited by 70% due to the antibiotic subsequently grew to higher densities than populations cultured without antibiotic (Supplementary Figure S13). Whole genome sequencing (WGS) of high K populations indicated the appearance, and partial sweep, of duplications of a genomic region containing a doxycycline efflux pump operon³⁷, *acr* (at frequencies 21, 25 and 42% in each of three replicates; Fig. 7 and Supplementary Fig. S15). It is on the basis of there being more cells with more efflux operons that we claim antibiotic resistance by efflux has increased in these populations, consistent with observations of increased r and K in the presence of doxycycline (Fig. 6 and Supplementary Fig. S13). WGS showed the excision of prophage *dlp12* from the AG100 genome at high frequency in high K populations (at frequencies 78, 84 and 88%). Polymorphisms common to all the drug-adapted populations observed at lower frequency were found in the insertion sequence (IS5) transposase, *insH-5* and in the carbon starvation lipoprotein (*sdp*) that mediates acid resistance (Supplementary Tables S1 and S2).

Although r , yield, K and drug resistance increased, and rK improvements remained following drug withdrawal (Fig. 6), we were able to isolate a cost for this improvement: an increased duration of lag phase (Supplementary Fig. S14). It is notable that although doxycycline is said to be bacteriostatic³⁸, in fact here it stimulates biomass production while lengthening lag phase beyond 24 h without slowing exponential growth (Supplementary Fig. S14b). Thus, assays testing the antibiotic effect of doxycycline for 24 h, or less, can conclude that it reduces growth rate when, instead, it merely increases the waiting time to exponential growth.

Discussion

The logistic equation (8) is extremely useful when seeking growth rate and populations sizes of microbial growth data, but this does not mean rK selection theory provides any mechanistic insight into our data. Indeed, simply because the logistic model is a good fit of a growth data set, one cannot deduce that r and K trade-off, nor can one exploit that data fit to understand the nature of selection for r or K in that population. A range of theoretical and computational tools were required here to elucidate the selective forces in our experimental system. We needed mathematical models that causally relate growth efficiency, and therefore population size, to the rate of population growth and WGS data highlighted the likely cause of that efficiency increase. Here this amounts to selection for the amplification of an efflux pump and the loss of a prophage from the genome.

rK theory is consistent with our data sets where r and K are negatively correlated, for example in Fig. 1a, although any previous claim that r and K were correlated would have been consistent with our

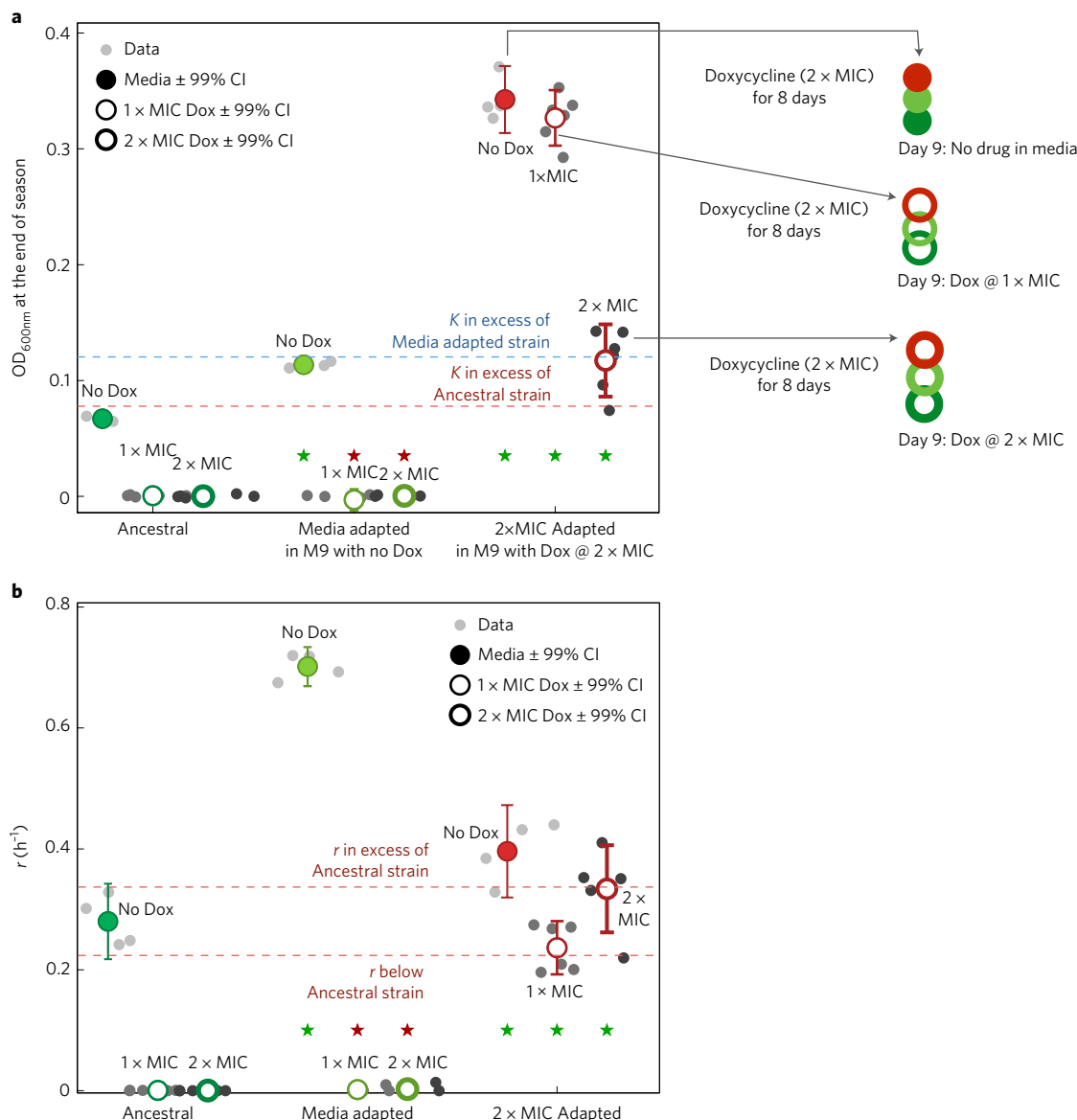


Figure 6 | Simultaneous rK-adaptation from an antibiotic challenge where drug resistance also increased. **a,b,** K (**a**; units of OD_{600nm}) and r (**b**) for three strains of *E. coli* K12(AG100) labelled ‘Ancestral’, ‘Media Adapted’ and ‘2 × MIC Adapted’ (Supplementary Methods describe protocols). The last two strains were derived from Ancestral by ~60 generations of adaptation to media containing either no antibiotic (then labelled Media Adapted) or else in two times the MIC of doxycycline (Dox; then labelled 2 × MIC Adapted); this is a clinical dose. All three strains were then cultured for 1 day (the ‘day 9’ data indicated) in media containing either no antibiotic (filled circle), a dose of doxycycline equivalent to the MIC (1 × MIC, thin open circle) or twice the MIC (thick open circle). We tested whether differences in K (**a**) and r (**b**) were significant (green star) or not (red star) with respect to the Ancestral strain under identical day 9 conditions (t -test, $P < 0.05$ in each case). Unexpectedly, as shown in **a**, the greatest K was observed when ‘2 × MIC Adapted’ was cultured either in the absence of doxycycline or with doxycycline present at 1 × MIC. Unsurprisingly, as shown in **b**, the greatest r was observed when Media Adapted was cultured in media with no doxycycline; ‘2 × MIC Adapted’ had an r phenotype in the presence of doxycycline at a 2 × MIC concentration that could not be distinguished from Ancestral cultured in the absence of doxycycline; when doxycycline was withdrawn, the r of strain ‘2 × MIC Adapted’ was larger than Ancestral. Thus, drug-resistance adaptation has restored r above ancestral values while also increasing K .

data somewhere due to the humped, parabolic geometry we observe in rK and rate–yield data.

Ours is a laboratory study but there is a potential medical consequence of this geometry and the subsequent presence of rK trade-offs: mutations that overcome chemotherapies designed to reduce growth rate can also increase population size. Here, such adaptations created drug-resistant populations of bacteria that grow more quickly, and to higher densities, than bacteria not treated with antibiotics. These beneficial adaptations bear costs that are relevant to survival outside the laboratory. The doubling of lag time (Supplementary Fig. S14, ‘lag time’ is parameter L in equation (9)) means the evolved strains

can take twice as long to profit from increased nutrient uptake if the environment switches from a glucose-poor to a glucose-rich state. The loss of *dlp12* prophage removes protection from environmental stresses: *dlp12* is implicated in biofilm formation, an important aspect of the drug-resistance phenotype³⁹. The observed *acr* amplifications can be strongly selected against in environments without antibiotic⁴⁰. So, although a three-dimensional phenotype of (rate, yield, resistance) shows positively correlated adaptation in laboratory conditions, the five-dimensional phenotype (rate, yield, resistance, lag time, biofilm production) indicates that those changes come with costs that will be exposed in other environments.

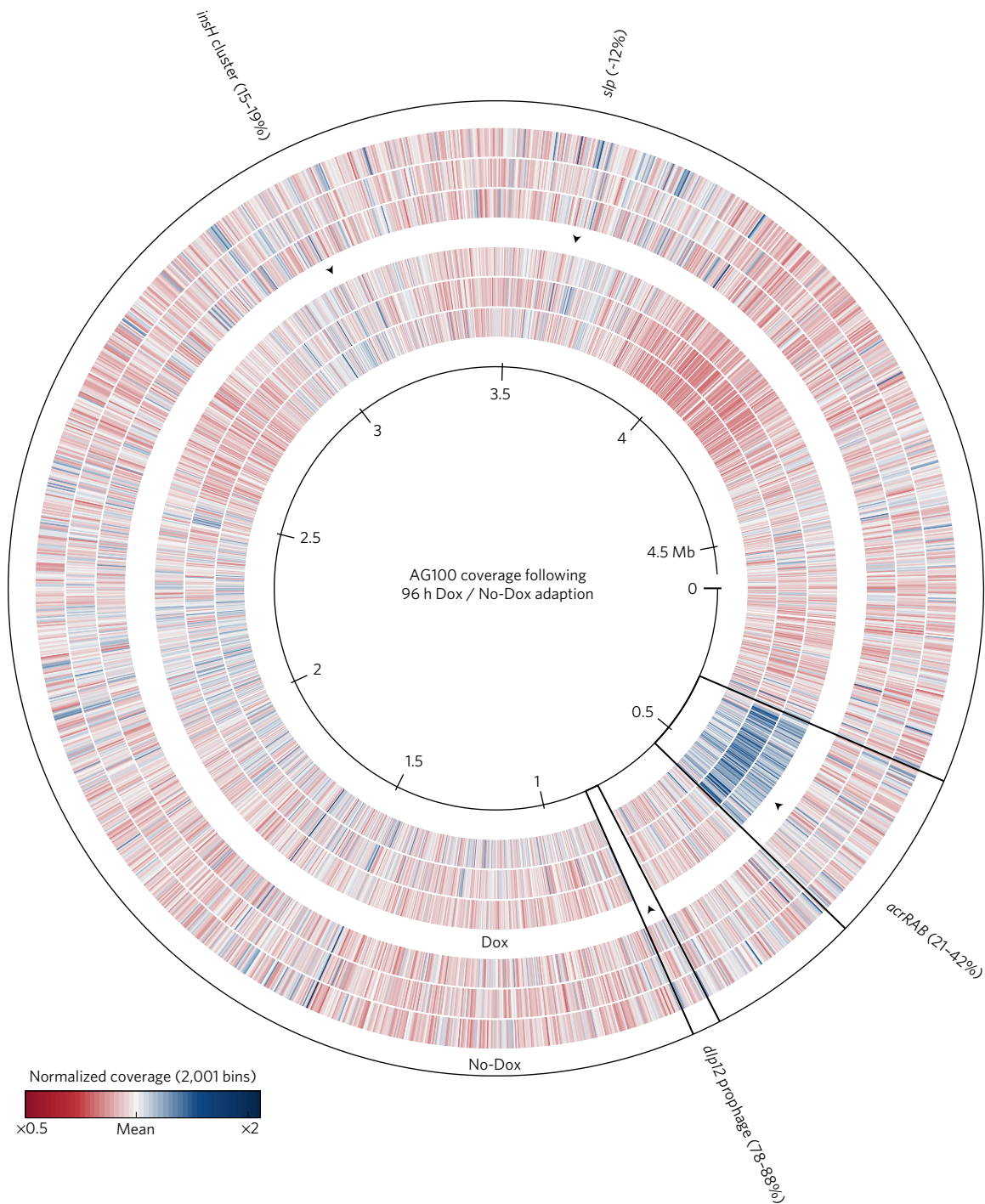


Figure 7 | A DNA coverage plot for *E. coli* K12(AG100) following ~60 generations (96 h) of growth in the presence and absence of doxycycline. Data in the presence (three inner annuli, 'Dox') and absence (three outer annuli, 'No-Dox') indicate potential genetic mechanisms supporting positive r , K and resistance adaptation. A change in DNA detected in the sequencing protocol is shown in red (reduction) and blue (increase; and white is complete loss), respectively, with respect to no mean change (in grey). The inner ring (black) indicates genome position and three replicates for each treatment were sequenced (indicated in Supplementary Fig. S13). The white region marked *dlp12* shows the deletion of prophage *dlp12* only during doxycycline treatment. The outer text labels summarize the estimated frequencies of mutations common to all three replicate populations, indicating positive selection for the doxycycline efflux operon, *acr*, with the prophage deletion at even higher frequency.

Finally, it is possible that the humped rK geometry we observe applies to tumours and metazoa because equations (6) and (7) were derived from a theoretical model of a branched, glucose-processing pathway¹⁰ common to all living cells. However, those equations are not applicable when different cells express those pathways differently or do not have pathways in common.

Therefore, to generalize our findings to such heterogenous populations, one could extend equations (6) and (7) to a situation where one microbial strain uses an extracellular, secondary metabolite of another microorganism to grow. We hypothesize, in such a microbial community, that r , yield and K will also exhibit positive correlations.

Methods

The Supplementary Information contains additional details on the methods used to analyse data.

Throughout, estimates of r and K are obtained from microbial growth data using the logistic equation

$$\frac{dN}{dt} = rN(1 - N/K), \quad x(0) \geq 0 \quad (8)$$

whose solutions are modified to account for lag phase, where dN/dt is the microbial per capita growth rate. This means r , K and L are determined from the best fit of the following four-parameter model to microbial density time series:

$$N(t) = \beta + \frac{K}{1 + q \times e^{-r(t-L)}} \quad (9)$$

where $N(t)$ is density at time t . In this model, β is the estimated experimental blank, needed because microtitre plates used for culture absorb light, q is a composite parameter that contains the initial population size, $N(0)$, and L is lag, a proxy for the time taken for growth to enter exponential phase. Yield is calculated as the ratio between K and the glucose supplied to the growth medium (Supplementary Figs S1 and S2).

Please note that the biological parameter L is used throughout the text and Supplementary Information, and is always referred to by the term 'lag'. The parameter β is not a biological phenotype. It is an electromechanical parameter associated with the microtitre plates and plate-reading devices in which microbial population densities are measured. It refers to a constant measure of the light absorbance of the material from which those plates are constructed and the value of β derives from that material, in addition to the light absorbed by the liquid media placed in each well of the plate that allows microbial cultures to grow. This value must be properly subtracted from optical density readings to determine microbial population densities and the definition of $N(t)$ above allows us to do this in a reliable manner that accounts for potential errors in estimates of β . The parameter β might be termed the 'blank' but this term is used nowhere in the paper.

The parameters associated with equation (8) are estimated by fitting equation (8) to microbial growth data using NonLinearModel.fit in Matlab. This is a powerful nonlinear regression facility that produces a range of statistics on the robustness and suitability of that fit to the data set in question. Once estimates of r and K have been obtained, with associate uncertainties, because glucose has been supplied to the cells at a controlled concentration, S_0 , the efficiency of biomass production is the value K/S_0 .

Microbial biomass measure. Throughout our empirical work, we use optical density (OD) as a proxy for biomass. Our reasons for doing so are (1) OD is known to correlate well with live cell counts at the densities we are using, see the supplementary information in these references^{10,37}; (2) OD accounts for mass contained in non-viable cells that have previously sequestered carbon from the environment and therefore count as biomass, even if they no longer grow; and (3) OD need not always correlate with live cell counts because cell size changes are accounted for within OD (larger cells produce a larger OD for equivalent population sizes), but this is consistent with the use of OD as a proxy for biomass; indeed, larger cells will have sequestered more carbon from the extracellular environment than smaller cells.

Other measures could be used as a proxy for biomass, and therefore yield (that is, efficiency: biomass produced per carbon supplied), for example (1) colony forming units (that is, live cells counts); (2) total cell count performed by flow cytometry; (3) total DNA; and (4) dry mass. We chose OD as it can be measured on a minute-by-minute basis for large numbers of replicates and culture conditions, allowing us to measure dynamics in the chosen biomass measure without disrupting or sampling the culture vessel, something that is not readily feasible for the other measures mentioned here.

C. glabrata rK data using 24 h cultures. Overnight cultures were prepared in yeast peptone dextrose medium with 20 mg ml⁻¹ glucose (2% w/v) in 4 ml volumes in universal tubes, via inoculation of a single colony per tube. Following 18–24 h incubation at 30 °C and 180 r.p.m., overnights were centrifuged and washed once in PBS solution prior to resuspension in synthetic complete (SC) minimal medium at the appropriate glucose concentration. SC medium was prepared at 14 different glucose concentrations (0.25–32 mg ml⁻¹) via autoclaving of media components (excluding glucose and 10% of the final media volume) prior to the addition of filter-sterilized glucose solution. D-glucose was dissolved in distilled, de-ionized water to reach a final concentration of 320 mg ml⁻¹ (32% w/v) and sterilized through a 0.22 µm filter unit. Glucose was diluted appropriately in autoclaved SC media water used to produce a final volume as required to prepare SC media with 4, 12, 20, 24 and 32 mg ml⁻¹ glucose concentrations. All other SC media were prepared from a 200 mg ml⁻¹ (20% w/v) glucose stock solution. These experiments were repeated in triplicate.

E. coli rK data from 24 h/48 h cultures. A volume of 150 µl of M9 minimal media was prepared using dilute K₂HPO₄ (350 g), KH₂PO₄ (100 g) in 1 L of de-ionized water, and dilute trisodium citrate (29.4 g), (NH₄)₂SO₄ (50 g) and MgSO₄ (10.45 g) in 1 l of de-ionized water, autoclaved and diluted accordingly. Filtered, sterilized glucose and casamino acids were added from a 20% w/v stock. All strains were grown in M9 minimal media supplemented with 0.1% casamino acids and glucose ranging from 0 to 3 mg ml⁻¹, incubated at 30 °C and shaken in a Tecan Infinite Pro for 24 h with reads taken every 20 min. Inoculating strains (AG100, MG1655 and *rrn* operon knockouts derived from MG1655) were prepared from overnight cultures in liquid LB medium, grown in M9 supplemented with 0.125 mg ml⁻¹ of glucose and centrifuged prior to inoculation. These experiments were replicated six times.

E. coli K12(AG100, MG1655 and *rrn* operon knockouts) antibiotic adaptation protocols. For extended doxycycline and no-doxycycline control treatments at 30 °C, a microtitre plate reader measured OD_{600nm} of cultured bacteria every 20 min in 96-well microtitre plates containing 150 µl of liquid M9 medium supplemented with glucose (0.2%) and casamino acids (0.1%), both with and without antibiotics. All cultures were shaken in a linear manner before each OD measurement. Inoculating *E. coli* were taken from a colony and cultured overnight in M9 (0.2% glucose, 0.1% casamino acids). At the end of either 12 h or 24 h, called the length of a 'season', a 96-pin replicator was used to transfer a 1% of volume sample (the volume transferred is approximately 1.5 µl) to a new plate containing fresh growth medium and antibiotics, thus creating a new season of growth. The same environment was maintained for each subsequent transfer (eight seasons of treatment in total) and each replicate population (repeated in triplicate). The resulting OD time series were imported into Matlab R2013b to subtract the background (blank wells containing only medium) and generate all other statistics described here.

Based on the 24 h data in Supplementary Fig. S12, the MIC of *E. coli* AG100 when exposed to doxycycline was taken as 0.6 µg ml⁻¹ for the purposes of this study. This is also called 1 × MIC in the main text and 2 × MIC is twice this concentration. When treatments of AG100 are said to be 'sub-MIC' in the main text, the doxycycline concentration was 0.2 µg ml⁻¹ (see Supplementary Fig. S12) and this achieves a reduction in population size over a 24 h period of AG100 growth that approximately equates to a 70% inhibition relative to the same *E. coli* strain cultured in the absence of doxycycline.

Sequencing and bioinformatics protocols. *Genetic mechanisms of adaptation in antibiotic-evolved populations of E. coli* (AG100). To determine genetic mechanisms that might account for the *K*-stimulatory effect of the antibiotic doxycycline on AG100 reported in the main text, we sequenced the genomes of three evolved populations from the treatment that resulted in the highest cell density (measured by OD). These are indicated in Supplementary Fig. S13. To ensure the genetic changes were the result of antibiotic challenge, we also sequenced three control populations from that figure that evolved under experimental conditions but were not exposed to any antibiotics. We further sequenced three replicates of the ancestral population to ensure conformity between our starting strain and the published AG100 reference.

DNA extraction. DNA was extracted from frozen samples (150 µl culture + 75 µl 80% glycerol); a small quantity (<1 µl) was removed from the frozen population in a microtitre plate well using a sterile tip and inoculated into M9 media containing the same concentration of nutrients and antibiotic as the adaptive condition in that microtitre well, therefore recapitulating the conditions of season 8 in Supplementary Fig. S13. DNA was extracted using an Ambion geneJET DNA extraction kit following the manufacturer's instructions, with an additional ethanol wash step, and additional elution step to maximize DNA purity and yield. Samples were extracted from populations taken from season 8. DNA was also processed on a 1% agarose gel to ensure that DNA size was in excess of 10,000 bp and to ensure that there was no protein contamination. DNA was accurately quantitated using the Qubit system, ensuring yields of more than 25 ng µl⁻¹ in 50 µl. Paired-end DNA libraries were prepared by Exeter Sequencing Service, using the Nextera (Illumina) library preparation protocol.

DNA quality control and mapping. Reads were trimmed using FASTQC to ensure a mean phred score of at least 25 at all positions of the read. Adapter sequence trimming was performed by ESS. All sample reads were mapped to a previously published *E. coli* K12(AG100) reference genome available for download at the website mentioned in the 'Annotation' section below.

Each sequence was indexed to the reference in fasta format using the Burrows-Wheeler alignment (BWA) index subroutine (BWA 0.7.4). Alignment was also performed using BWA and aligned files were subsequently sorted into genomic position and indexed using Samtools, and filtered to remove any non-paired end matches. Coverage was analysed using genomeCoverageBed in BEDTools⁴¹ and data were further analysed in Matlab.

Variant calling. Single nucleotide polymorphisms (SNPs) were called using VarScan 2.3.8. VarScan uses a heuristic method based on read depth, base quality

and variant frequency to call SNPs. Filters were added to SNP calling to ensure that high-quality calls were made. These quality filters were a minimum read depth of 60, with at least 10 reads supporting the alternative variant, a *P* value of 0.05 or less and a minimum average quality of 30. Additionally, VarScan calls SNPs as homologous if more than 90% of the reads support one or the other variant. VarScan also detected short indels in the same manner. Pindel was used to detect structural variations, including inversions, rearrangements and indels. Pindel works by detecting breakpoints using a pattern-growth algorithm. This identifies paired reads whereby only one of the reads is able to map to the reference. By breaking the unmapped read into shorter fragments, and re-mapping, the breakpoint of insertions or deletions can be detected. Duplication events were determined using CNVnator v0.3, with a bin size of 100, and Matlab, using coverage data from BEDTools.

Annotation. Annotation files from the previously published AG100 genome were used in annotation of WT populations of AG100. These files were accessed from EBI (<http://www.ebi.ac.uk/ena/data/view/PRJEB7832>).

Annotation of the evolved genomes was also performed using RAST for initial web-based viewing, and PROKKA to annotate the consensus fasta files of all experimental replicates.

Clustering analysis. Given r and K data taken from replicated culture experiments using several genetically distinct strains of *E. coli*, we require a rationale to decide which strain optimizes r and K . Rather than use multiple pairwise comparisons, instead we used an agglomerative clustering approach to categorize the whole phenotypic data set, r and K , into some number of clusters that represent subsets of the entire data set with similar phenotype. A natural prior expectation is that the data from a single genotype are found within one phenotypic cluster, although one such cluster may contain the data of two, or more, genotypes. With this in mind, we used the following algorithm to determine the genotype that maximizes the phenotypes r and K .

First, choose a clustering algorithm that takes a data set D and returns a categorization of this data set as i distinct clusters, call it $C(i,D)$. Now, given n genotypes and a phenotypic r data set, R , to categorize, for all $i = 2, \dots, n$ from the output $C_i = C(i,R)$. Let $R(\cdot)$ be the function that returns the set of phenotypic values for a given cluster.

We call a cluster viable, with parameter p , if a one-way ANOVA is unable to detect significant differences, at level p , between all phenotypes in that cluster, this is, the set $R(C(i,R))$. The entire clustering is said to be admissible if each cluster is itself viable and, moreover, the phenotypes from any two distinct clusters can be detected by testing with a one-way ANOVA at significance level p , thus $R(C(i,R))$ and $R(C(j,R))$ represent significantly different sets of phenotypic values for $i \neq j$.

Then, for each admissible clustering, i^* , choose the cluster label, $m(i^*) \in \{1, \dots, i^*\}$, which contains the maximal phenotype max $R \in R(C_{m(i^*)})$. The optimal genotypes are said to be all those found within $C_{m(i^*)}$.

The clustering method, C , used for Fig. 5b is an agglomerative, one-dimensional clustering analysis that was performed on the *rrn* operon mutants for both growth rate (r) and carrying capacity (K) data sets. To implement this, we used the routines *clusterdata* and *anova1*, as implemented in Matlab 2013a, whereby $i^* = 3$ was determined to be the number of admissible clusters in each case when $P = 0.05$.

For the K data set, the cluster of optimal genomes corresponding to $\{3, 4, 5\}$ (and these values are the numbers of *rrn* operons present in the genome) were deemed to be optimal according to the above algorithm, whereas $\{3, 4, 7\}$ was the analogous set determined for the r data set. The intersection of these two sets is $\{3, 4\}$, which we therefore deem to be the optimal pair of strains (that is, *rrn* strains $\Delta 3$ and $\Delta 4$) in the sense that these may both be said to maximize r and K across the entire data set studied here.

Data availability. Data for figures that do not use genome sequence data are available in Excel spreadsheet format at <http://people.exeter.ac.uk/reb217/rebHomePage/data.html> (this link also contains coarse-grained DNA coverage data used in Fig. 7). A complete whole genome sequencing data set can be accessed at <http://www.ebi.ac.uk/ena> using ENA project accession number [PRJEB15352](#). Please email the corresponding author to request any of the Matlab scripts used in this work.

Received 7 June 2016; accepted 9 December 2016;
published 30 January 2017

References

- Herron, M. D. & Doebeli, M. Parallel evolutionary dynamics of adaptive diversification in *Escherichia coli*. *PLoS Biol.* **11**, e1001490 (2013).
- Maharjan, R. *et al.* The form of a trade-off determines the response to competition. *Ecol. Lett.* **16**, 1267–1276 (2013).
- Ben-Hur, E., Fragman-Sapir, O., Hadas, R., Singer, A. & Kadmon, R. Functional trade-offs increase species diversity in experimental plant communities. *Ecol. Lett.* **15**, 1276–1282 (2012).
- Kraaijeveld, A. R. & Godfray, H. C. Trade-off between parasitoid resistance and larval competitive ability in *Drosophila melanogaster*. *Nature* **389**, 278–280 (1997).
- Fine, P. V. A. *et al.* The growth-defense trade-off and habitat specialization by plants in Amazonian forests. *Ecology* **87**, S150–S162 (2006).
- Dieckmann, U. & Doebeli, M. On the origin of species by sympatric speciation. *Nature* **400**, 354–357 (1999).
- Calsina, A. & Quadrado, S. Small mutation rate and evolutionary stable strategies in infinite dimensional adaptive dynamics. *Math. Biol.* **48**, 135–159 (2004).
- Metz, J. A. J., Geritz, S. A. H., Meszena, G., Jacobs, F. J. A. & Van Heerwaarden, J. S. in *Stochastic and Spatial Structures of Dynamical Systems* (eds van Strien, S. J. & Verdun Lunel, S. M.) 183–231 (North Holland, 1996).
- Gudelj, I., Coman, C. D. & Beardmore, R. E. Classifying the role of trade-offs in the evolutionary diversity of pathogens. *Proc. R. Soc. A* **426**, 97–116 (2006).
- Meyer, J. R., Gudelj, I. & Beardmore, R. Biophysical mechanisms that maintain biodiversity through trade-offs. *Nat. Commun.* **6**, 6278 (2015).
- Beardmore, R. E., Gudelj, I., Lipson, D. A. & Hurst, L. D. Metabolic trade-offs and the maintenance of the fittest and the flattest. *Nature* **472**, 342–346 (2011).
- Reznick, D., Nunney, L. & Tessier, A. Big houses, big cars, superfleas and the costs of reproduction. *Trends Ecol. Evol.* **15**, 421–425 (2000).
- Leiby, N. & Marx, C. J. Metabolic erosion primarily through mutation accumulation, and not tradeoffs, drives limited evolution of substrate specificity in *Escherichia coli*. *PLoS Biol.* **12**, e1001789 (2014).
- Lipson, D. A. The complex relationship between microbial growth rate and yield and its implications for ecosystem processes. *Front. Microbiol.* **6**, 615 (2015).
- Mueller, L. D. & Ayala, F. J. Trade-off between *r*-selection and *k*-selection in *Drosophila* populations. *Proc. Natl Acad. Sci. USA* **78**, 1303–1305 (1981).
- Sibly, R. M. & Hone, J. Population growth rate and its determinants: an overview. *Phil. Trans. R. Soc. Lond. B* **357**, 1153–1170 (2002).
- Luckinbill, L. S. *r* and *K* selection in experimental populations of *Escherichia coli*. *Science* **202**, 1201–1203 (1978).
- Luckinbill, L. S. Selection and the *r/K* continuum in experimental populations of protozoa. *Am. Nat.* **113**, 427–437 (1979).
- Nilsson, A. I. *et al.* Reducing the fitness cost of antibiotic resistance by amplification of initiator tRNA genes. *Proc. Natl Acad. Sci. USA* **103**, 6976–6981 (2006).
- Millan, A. S. *et al.* Positive selection and compensatory adaptation interact to stabilize non-transmissible plasmids. *Nat. Commun.* **5**, 5208 (2014).
- Blair, J. M. A. *et al.* AcrB drug-binding pocket substitution confers clinically relevant resistance and altered substrate specificity. *Proc. Natl Acad. Sci. USA* **112**, 3511–3516 (2015).
- Stearns, S. *The Evolution of Life Histories* (Oxford Univ. Press, 1992).
- Aktipis, C. A., Boddy, A. M., Gatenby, R. A., Brown, J. S. & Maley, C. C. Life history trade-offs in cancer evolution. *Nat. Rev. Cancer* **13**, 883–892 (2013).
- Korolev, K. S., Xavier, J. B. & Gore, J. Turning ecology and evolution against cancer. *Nat. Rev. Cancer* **14**, 371–380 (2014).
- Pfeiffer, T., Schuster, S. & Bonhoeffer, S. Cooperation and competition in the evolution of ATP-producing pathways. *Science* **292**, 504–507 (2001).
- Novak, M., Pfeiffer, T., Lenski, R. E., Sauer, U. & Bonhoeffer, S. Experimental tests for an evolutionary trade-off between growth rate and yield in *E. coli*. *Am. Nat.* **168**, 242–251 (2006).
- Wong, W. W., Tran, L. M. & Liao, J. C. A hidden square-root boundary between growth rate and biomass yield. *Biotechnol. Bioeng.* **102**, 73–80 (2009).
- Fitzsimmons, J., Schoustra, S., Kerr, J. & Kassen, R. Population consequences of mutational events: effects of antibiotic resistance on the *r/k* trade-off. *Evol. Ecol.* **24**, 227–236 (2010).
- Mori, M., Hwa, T., Martin, O. C., De Martino, A. & Marinari, E. Constrained allocation flux balance analysis. *PLoS Comput. Biol.* **12**, e1004913 (2016).
- Stearns, S. C. The evolution of life history traits: a critique of the theory and a review of the data. *Annu. Rev. Ecol. Syst.* **8**, 145–171 (1977).
- Monod, J. The growth of bacterial cultures. *Annu. Rev. Microbiol.* **3**, 371–394 (1949).
- Roughgarden, J. Density-dependent natural selection. *Ecology* **52**, 453–468 (1971).
- Boyce, M. S. Restitution of *r*- and *k*-selection as a model of density-dependent natural selection. *Annu. Rev. Ecol. Syst.* **15**, 427–447 (1984).

34. MacLean, R. C. & Gudelj, I. Resource competition and social conflict in experimental populations of yeast. *Nature* **441**, 498–501 (2006).
35. Koch, A. R. & Deppe, C. S. *In vivo* assay of protein synthesizing capacity of *Escherichia coli* from slowly growing chemostat cultures. *J. Mol. Biol.* **55**, 549–562 (1971).
36. Stevenson, B. S. & Schmidt, T. M. Growth rate-dependent accumulation of RNA from plasmid-borne rRNA operons in *Escherichia coli*. *J. Bacteriol.* **180**, 1970–1972 (1998).
37. Fuentes-Hernandez, A. *et al.* Using a sequential regimen to eliminate bacteria at sublethal antibiotic dosages. *PLoS Biol.* **13**, e1002104 (2015).
38. Chopra, I. & Roberts, M. Tetracycline antibiotics: mode of action, applications, molecular biology, and epidemiology of bacterial resistance. *Microbiol. Mol. Biol. Rev.* **65**, 232–260 (2001).
39. Wang, X. *et al.* Cryptic prophages help bacteria cope with adverse environments. *Nat. Commun.* **1**, 147 (2010).
40. Laehnemann, D. *et al.* Genomics of rapid adaptation to antibiotics: convergent evolution and scalable sequence amplification. *Genome Biol. Evol.* **6**, 1287–1301 (2014).
41. Quinlan, A. R. & Hall, I. M. BEDTools: a flexible framework for comparing genomic features. *Bioinformatics* **26**, 841–842 (2010).

Acknowledgements

The *rrn* knockout strains derived from *E. coli* MG1655 were gifted by T. Bollenbach, strain AG100 was provided by S. Levy and *Candida* strains were a gift from S. Bates, who are sincerely thanked for their help.

Author contributions

R.B., I.G., M.H. and C.R.R. proposed research questions and hypotheses, and subsequently designed the experiments; R.B., C.R.R., F.G. and M.H. designed and wrote computer codes to analyse the data; C.R.R., M.H. and S.D. performed the experiments; and R.B., C.R.R. and I.G. wrote the manuscript.

Additional information

Supplementary information is available for this paper.

Reprints and permissions information is available at www.nature.com/reprints.

Correspondence and requests for materials should be addressed to R.B.

How to cite this article: Reding-Roman, C. *et al.* The unconstrained evolution of fast and efficient antibiotic-resistant bacterial genomes. *Nat. Ecol. Evol.* **1**, 0050 (2017).

Competing interests

The authors declare no competing financial interests.